



# Influence of dispersion media on Nafion® ionomer distribution in proton exchange membrane fuel cell catalyst carbon support

Raghunandan Sharma<sup>a</sup>, Laila Grahl-Madsen<sup>b</sup>, Shuang Ma Andersen<sup>a,\*</sup>

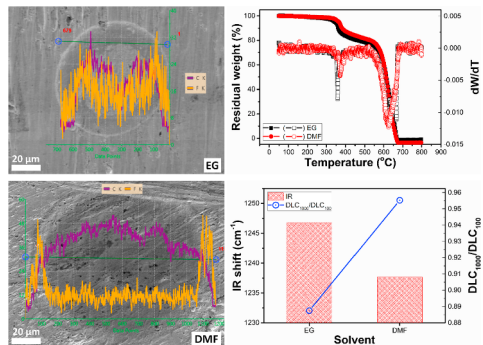
<sup>a</sup> Department of Chemical Engineering, Biotechnology and Environmental Technology, University of Southern Denmark, Campusvej 55, DK-5230, Odense M, Denmark

<sup>b</sup> EWII Fuel Cells A/S, Emil Neckelmanns Vej 15, 5220, Odense, Denmark

## HIGHLIGHTS

- Ionomer/support interface has been studied using electron microscopy and IR spectroscopy.
- Solvent used for catalyst ink formation affects the interface significantly.
- The change of DLC with scan rate and the IR shifts for ionomer show significant correlations.

## GRAPHICAL ABSTRACT



## ARTICLE INFO

### Keywords:

Interface  
Solvent  
Spectroscopy  
Double layer capacitance (DLC)  
PEMFCs

## ABSTRACT

Interface between the Nafion® ionomer on the high surface area carbon used as catalyst support in the polymer electrolyte membrane fuel cell (PEMFC) electrodes has been studied through a combination of microscopic, spectroscopic and electrochemical techniques. Different support/ionomer interface structures have been developed by varying the dispersion media for ink preparation while keeping the solid composition of the ink invariant. Structural characterizations such as elemental mapping, thermogravimetric analysis and Raman/Infrared spectroscopy of the dried inks reveal significant impact of the dispersion media on the distributions of the ionomer/support phases. Further, variation of the double layer capacitance (DLC) of the ionomer/support inks coated on gold electrodes with the scan rate during cyclic voltammetry measurements has been studied to evaluate the ionomer/support interface performance. Substantial impact of the dispersion media has been observed on the scan rate/DLC profiles for the inks. Low ratios of the DLC values at scan rates of 1000 and 100 mV/s have been observed for the ionomer/carbon support inks having partially inhomogeneous ionomer/carbon distribution. Finally, infrared spectroscopy suggested different interactions of the  $-SO_3$  group with the support carbon for the inks prepared using different types of dispersion media.

## 1. Introduction

Highly efficient and cost-effective electrocatalysis of oxygen

reduction reaction (ORR)/hydrogen oxidation reaction (HOR) at cathode/anode of the polymer electrolyte membrane fuel cells (PEMFCs) is key to the large-scale applications of these highly efficient

\* Corresponding author.

E-mail address: [mashu@kbm.sdu.dk](mailto:mashu@kbm.sdu.dk) (S.M. Andersen).

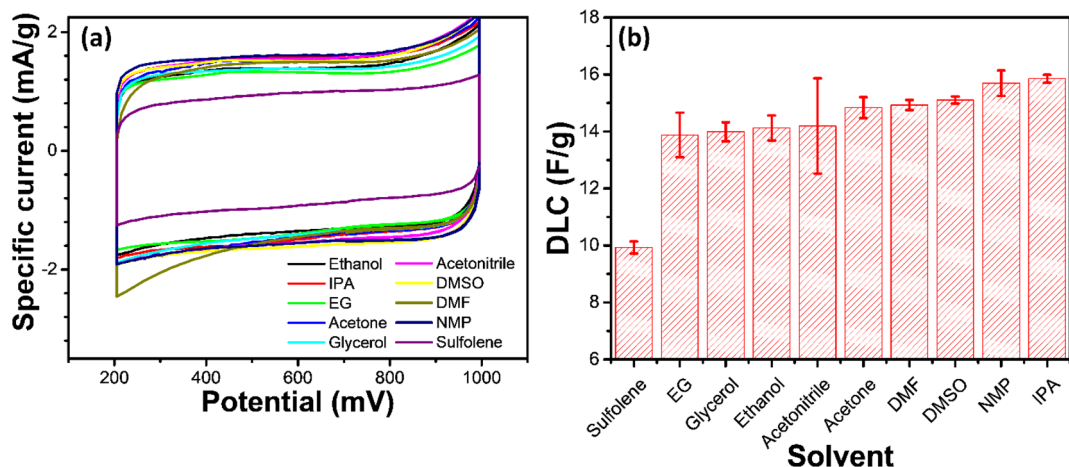


Fig. 1. (a) Cyclic voltammograms in N<sub>2</sub> saturated 1.0 M H<sub>2</sub>SO<sub>4</sub> and (b) variations of DLC for the ionomer/catalyst support inks prepared using different solvents.

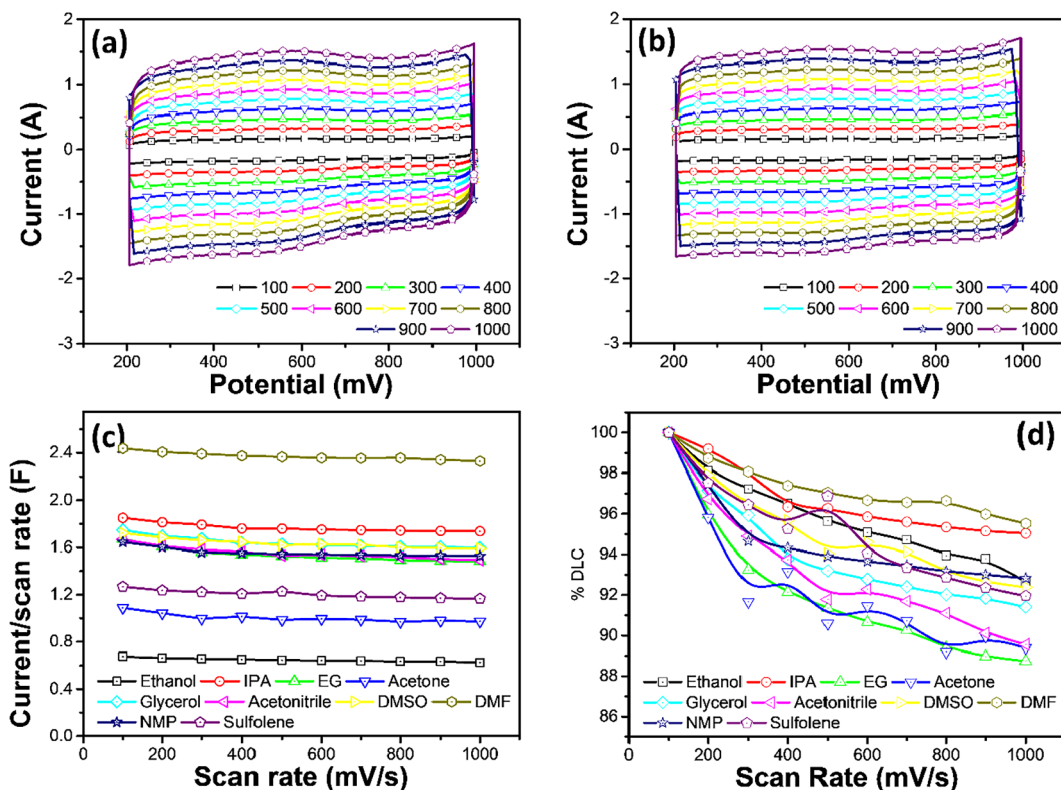


Fig. 2. (a–b) Representative cyclic voltammograms of catalyst support/ionomer ink coated gold electrodes in 1 M H<sub>2</sub>SO<sub>4</sub> at different scan rates for (a) EG and (b) NMP solvents. (c) Anodic current at 0.5 V/scan rate for the ionomer/catalyst support inks prepared using different solvents (not normalized to the ink loading). (d) Variations of relative DLC with potential scan rate for the ionomer/catalyst support inks prepared using different solvents.

and environmentally friendly energy conversion devices. PEMFC catalyst layers consist of nanoparticulate Pt or Pt-alloy catalysts supported on high surface area supports having high corrosion resistance and high electronic conductivity [1–5]. Significant efforts made towards development of PEMFC catalysts with low cost and high durability have witnessed a considerable reduction of required Pt-loading along with improved performance [6,7]. However, there is still room for improvement both in terms of catalyst loading, utilization and durability under the PEMFC working conditions [8,9].

Structure of the catalyst layer, i.e. the interfaces between various phases (catalyst particles, proton conducting phase and electron conducting phase) affect the electrode performance significantly [10–21]. The catalyst/support interface and the catalyst/ionomer interface,

being responsible for the conduction of the electrons and the protons in the PEMFC catalyst layer respectively, need to be optimized such that proper electron and the proton accessibility to the catalyst particles is insured. Impressive advancements towards understanding the nature of catalyst/ionomer interface and its influence on the catalyst layer performance have been made recently [22,23]. Previous studies performed in our group have shown significant impact of catalyst/ionomer interface on durability of Pt-based catalysts [10,24].

PEMFC electrodes in membrane electrode assembly (MEA) consist of catalyst layers coated either on polymer electrolyte membrane (PEM) or gas diffusion layer (GDL) and sandwiched between the both through hot pressing. Catalyst inks, prepared by dispersing the supported PEMFC catalyst and the ionomer in a suitable solvent are used to coat

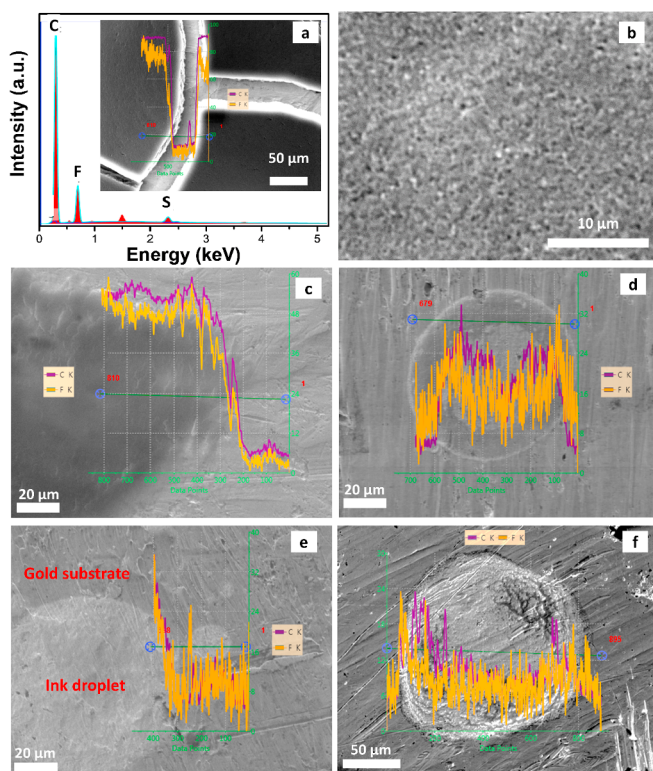


**Fig. 3.** (a) Typical EDX spectrum of the ionomer/catalyst support ink exhibiting characteristic peaks corresponding to C, F and S Inset shows a cracked film on gold electrode along with corresponding EDX line mapping. (b) SEM image of ink drop (solvent: IPA) showing uniform distribution of carbon/ionomer. SEM images and corresponding EDX line mapping of ink drops sprayed on gold surfaces for the inks prepared using different solvents, namely (c) IPA, (d) EG, (e) glycerol and (f) ethanol.

the catalyst layers through techniques such as spraying, decal transferring, ultrasonic spraying, brushing, screen-printing, etc. [17,25–28]. For a catalyst layer with particular Pt/C and ionomer contents, the nature of catalyst ink (solvent, solid content, state of dispersion, etc.) can play a significant role to determine the catalyst/ionomer interface, as revealed by studies performed on the effect of such parameters. Dispersion of the ionomer with the PEMFC catalysts (Pt/C) is affected by parameters such as wettability of the Pt/C catalyst. Profound effect of the ionomer agglomerate morphology on the catalyst performance has been found by Kim et al. by using different solvents for catalyst ink preparation [17]. However, owing to large surface area of the catalyst support, the catalyst/ionomer interface may be affected significantly by the support/ionomer interaction. Arrangement of the ionomer segments in a catalyst layer and hence the catalyst/ionomer interface may be altered through varying the surrounding chemical environment of the catalyst support and the ionomer phases during vaporization of solvents. Therefore, studies involving support/ionomer interactions could be quite informative towards understanding of the catalyst/ionomer interface in a PEMFC catalyst layer.

Generally speaking, electrochemical reactions [29] happen when (1) reagents approach and adsorb to the electrode surface, (2) charge transfer between the reactants and the electrode, and (3) the resulting product desorbs and leaves the electrode surface. This indicates the overall reaction rate can be either electron transfer dominated or mass transfer dominated. Many pioneer studies have been devoted to electrocatalysis to understand and improve charge transfer related reaction kinetics [30–35]. However, the rate of electron transfer through the electrode/electrolyte interface, the ionic/electronic conductivity, and the rate of reactant/product transport also govern the overall reaction rate [22,36]. This is especially true in high surface area porous gas

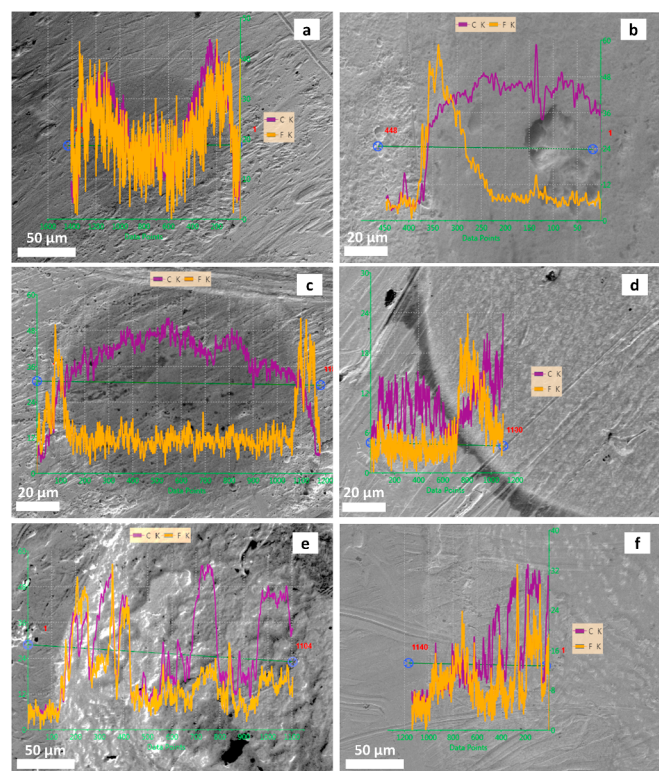


**Fig. 4.** SEM images and corresponding EDX line mapping of ink drops sprayed on gold surfaces for the inks prepared using different solvents, namely (a) sulfolene, (b) DMSO, (c) DMF, (d) NMP, (e) acetonitrile and (f) acetone. The EDX line mapping of C and F (normalized intensities) along the line shown on the image have also been embedded.

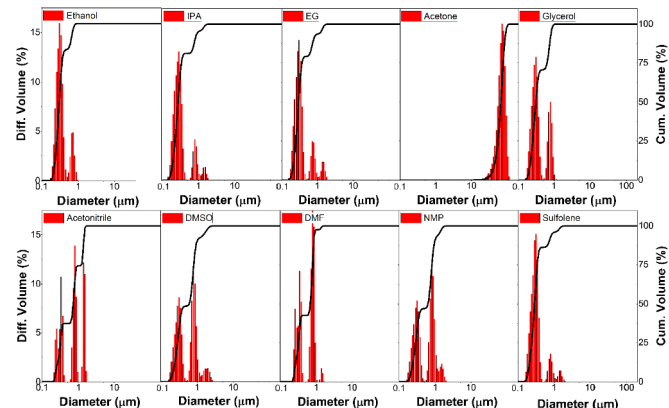


**Fig. 5.** Particle size distributions in terms of differential and cumulative volume % of the ionomer/catalyst support inks prepared using different solvents (shown in legends).

diffusion electrodes of complex component interactions and mass transport properties.

In the present study, an attempt has been made to investigate the ionomer/support interface structure with electric double layer capacitance (DLC) at different scan rates. The DLC measurement utilizes ion adsorption on the electrode surface without involving Faradaic electron transfer reaction, which is a relative fast process. The electrode surface under investigation is of high roughness and hydrophobicity, which is highly likely to encounter diffusion barriers. Therefore, the electrode reactions are mainly mass transport dominated. Persistence of the DLC in relation to the scan rate can reflect valuable information such as thickness of the diffusion layer, tortuosity of the porous structure and continuity of the electrode components.

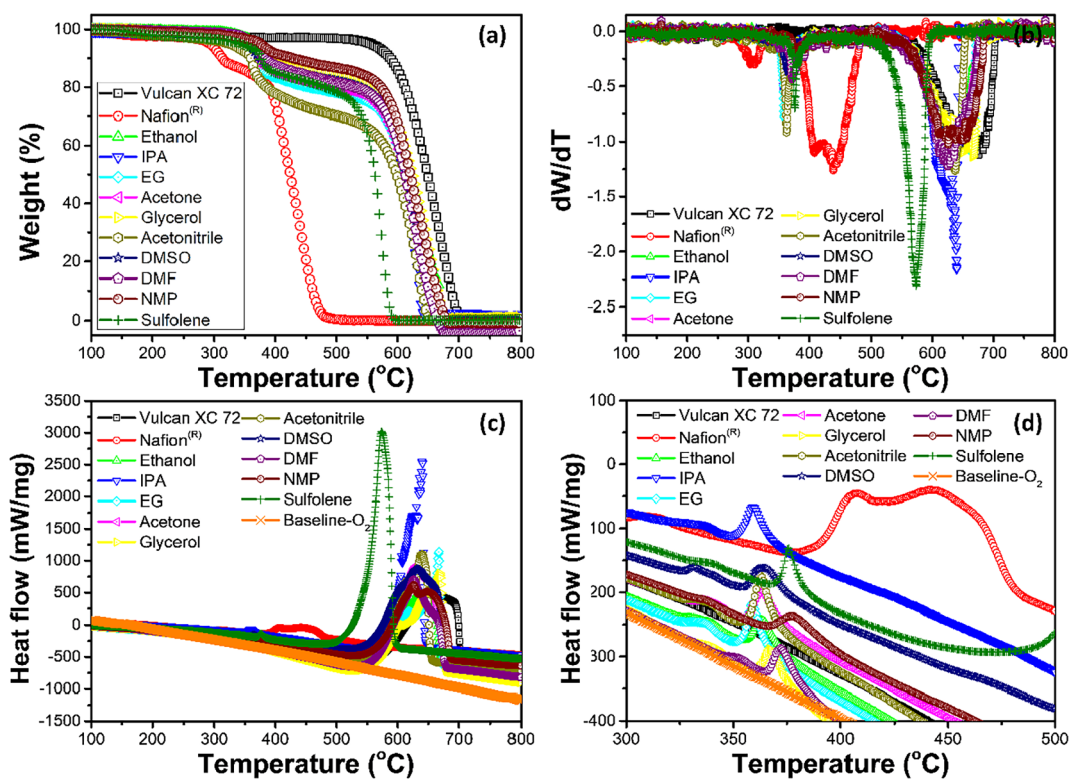


**Fig. 6.** Thermal degradation behavior of the Nafion ionomer, the Vulcan XC 72 carbon and the ionomer/catalyst support inks prepared using different solvents in presence of oxygen. TG, DTG and DSC plots have been shown in (a), (b) and (c), respectively, while (d) represents a magnified view of DSC plots for Nafion degradation region.

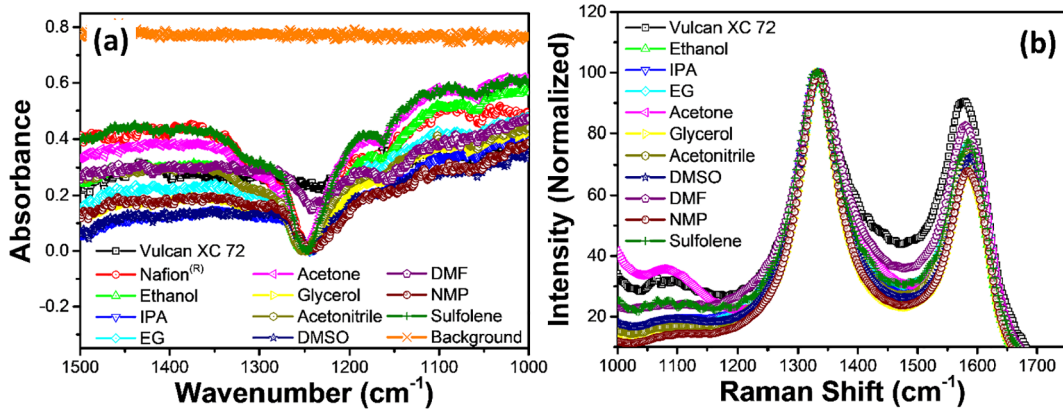


**Fig. 7.** (a) IR and (b) Raman spectra of Vulcan XC 72 carbon/Nafion® ionomer inks prepared using different solvents.

The focus of the current study is placed on the impact of solvent on the catalyst support/ionomer interaction on Vulcan® XC-72 carbon/Nafion (85:15 w/w) inks consisting of 3 wt% solid content prepared using 10 different solvents having large variations of physical/chemical properties. Correlation between the electric double layer capacitance (DLC) measured through voltammetry and the structural characteristics have been investigated to understand the impact of solvents on the support/ionomer interaction. The study reveals valuable information on catalyst support/ionomer interaction for electrode interface design.

## 2. Experimental methods

Catalyst inks were prepared using 10 different organic solvents (capable of dispersing/dissolving the ionomer), namely ethanol, isopropanol (IPA), ethylene glycol (EG), acetone, glycerol, acetonitrile, dimethyl sulfoxide (DMSO), dimethylformamide (DMF), N-Methyl-2-

pyrrolidone (NMP) and 2,5-dihydrothiophene 1,1-dioxide (sulfolene) by dispersing Vulcan® XC-72 carbon/Nafion (85:15 w/w) in a mixture of the organic solvent and milli-Q water (2/1 v/v). Vulcan® XC-72 carbon and Nafion ionomer (5 wt% Nafion solution; Ion Power, Dupont D521) were dispersed in the solvent mixture through ultrasonication (Hielscher UP200St) for 120 s to obtain typical inks of 3.0 wt% solid content with Vulcan®/Nafion weight ratio being 85/15. During ultrasonication, the glass vial containing the ink was kept cool using a water bath at 5 °C.

Electrochemical characterizations were performed by drop casting 5 µl of the ink (2.5 µl on each side) on a gold electrode consisting of an Au wire attached to an Au plate ( $2 \times 5 \text{ mm}^2$ ) and drying at 80 °C for 60–120 min (depending on the boiling point of solvent) in a vacuum oven. The carbon support loading on the gold electrode was estimated by weighing it before and after the ink coating using a quartz crystal microbalance (METTLER TOLEDO) with an accuracy of  $\pm 2 \mu\text{g}$ .

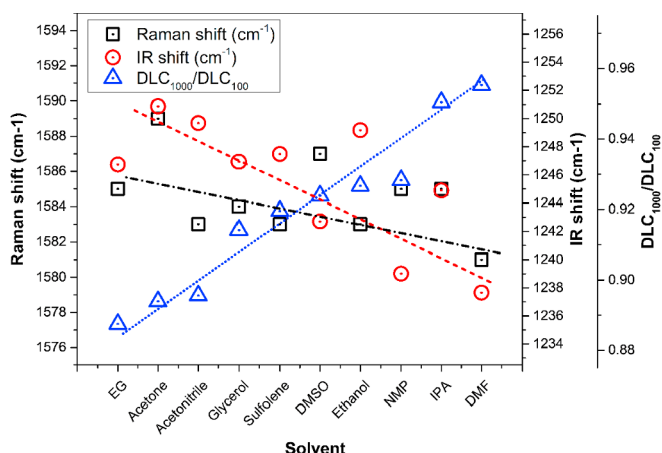


**Fig. 8.** Correlations between spectroscopic (Raman shift for carbon G-band and IR shift for the peak corresponding to  $-\text{SO}_3^-$  stretching of Nafion®) and the electrochemical (DLC<sub>1000</sub>/DLC<sub>100</sub>) parameters. Dashed lines are merely guide to eye.

Measurement of DLC was performed by using cyclic voltammetry (CV) in nitrogen saturated 1 M sulfuric acid electrolyte by a potential sweeping between 0.2 and 1.0 V vs reversible hydrogen electrode (RHE) at different scan rates varying between 100 and 1000 mV/s, after activating the electrodes by CV between 0.02 and 1.2 V at a scan rate of 100 mV/s for 20 cycles. The DLC was calculated using eq. (1), a simplified version of the standard equation described elsewhere [37].

$$\text{DLC} = \frac{I_a - I_c}{2\nu W_c} \quad (1)$$

Where,  $\nu$  is the scan rate,  $W_c$  is the ink loading on the electrode, while  $I_a$  and  $I_c$  are respectively the cathodic and anodic currents at 0.6 V, away from the Faradaic reactions.

Complete wetting of the support/ionomer ink coated on the electrolyte was ensured by dipping it in a ethanol/milli-Q water mixture (1/9 v/v) for ~30 s followed by rinsing with milli-Q water before the CV measurements using 1 M H<sub>2</sub>SO<sub>4</sub> electrolyte (H<sub>2</sub>SO<sub>4</sub>; EMSURE® grade, assay > 95–97%, Merck, Germany and milli-Q water; resistivity  $\geq 18.2 \text{ M}\Omega \text{ cm}$  at 25 °C) in Nitrogen atmosphere. The CV measurements were performed using graphite rod counter and Hg/Hg<sub>2</sub>SO<sub>4</sub> (REF 601 Radiometer®) reference electrodes. The experiments were repeated for three different electrodes for the reproducibility study.

Further, agglomeration state of the inks was examined through and particle size distribution (PSD) analysis using a LASER diffraction (single wavelength) Particle Size Analyzer (LS 13 320, Beckman Coulter) equipped with Universal Liquid Module. Structural characterizations such as simultaneous thermal analysis (thermogravimetric analysis (TGA) and differential scanning calorimetry (DSC)), infrared spectroscopy and scanning electron microscopy (SEM) including energy dispersive X-ray spectroscopy (EDX) were performed further by using the inks dried at 80 °C in vacuum oven. A NETZSCH STA449 F3 thermal analyzer was employed for the TGA and DSC measurement of the inks in presence of O<sub>2</sub> (1:3 mixture of O<sub>2</sub> and N<sub>2</sub>) at a heating rate of 5 °C/min. Fourier transform infrared (FT-IR) spectra of the inks were recorded using a Perkin Elmer 100 FT-IR Spectrometer. Samples were prepared by spraying thin layer of ink on an aluminium sheet as use of the dried ink powders or the spray coated ink on glass plate provided poor IR signal from ionomer due to the high absorbance of carbon. Microstructure and ionomer/catalyst support phase distribution were investigated by SEM imaging and EDX analysis through a Zeiss SEM equipped with a semiconductor X-ray detector operated at 20 kV. Samples for SEM/EDX analysis were prepared by spraying the inks gold substrates followed by vacuum drying. To observe any phase separation between support and ionomer during solvent drying, small drops of ink

prepared by air spraying it on gold plate followed by drying at 80 °C were analyzed through SEM imaging and EDX line mapping.

### 3. Results and discussion

#### 3.1. Electrochemical studies

Cyclic voltammograms (scan rate: 100 mV/s) of the inks (Normalized to the ink loading) shown in Fig. 1a exhibit characteristic double layer capacitor behavior with no Faradaic charge transfer peaks and a rectangle shape. Specific DLC (calculated from cathodic and anodic currents at 0.6 V) values for different inks show marginal variation except the relatively lower value for the ink prepared using sulfolene as solvent, probably due to its strong adsorption on the support carbon. High measurement uncertainty in case of acetonitrile may be attributed to the fact that the ink shows poor adhesion to the GC disc as portion of the catalyst layer (formed by drop casting followed by drying of the ink) was found detached from the GC disc. However, weight of these separated turnings has not been included in the measurement of the final loading of ink on electrode. The variation in specific DLC may be attributed to the varying electrolyte accessibility among the inks due to different ionomer/catalyst support distributions. However, due to the dependence of specific DLC on the ink loading and the electrode/ink adhesion, another approach was employed to study the ionomer/catalyst support interaction through measurement of relative change in DLC with scan rate, which may be considered less sensitive to the parameters such as the ink loading and the fraction of ink having no electronic connectivity.

Representative cyclic voltammograms of catalyst support/ionomer ink coated gold electrodes in 1 M H<sub>2</sub>SO<sub>4</sub> at different scan rates for EG and NMP solvents have been shown respectively in Fig. 2a and Fig. 2b. The voltammograms exhibit the characteristic capacitive shape even at high scan rates. Variations of anodic current at 0.5 V/scan rate (a quantity related directly to the DLC) for the inks prepared using different solvents have been shown in Fig. 3c, while the relative variations of DLC with scan rate (100 mV/s to 1000 mV/s) have been shown in Fig. 2d. With the increasing scan rate up to 1000 mV/s, the DLC was found to decrease heterogeneously depending on the nature of inks. Change of measured DLC with scan rate may be attributed to the decreased accessibility of the active electrode area for charge transfer and formation of double layer with increasing scan rate. Hence, difference in ionomer/interface structures should be reflected in the relative change of DLC with scan rate. A faster decrease of DLC with scan rate may be attributed to the higher hindrance to DLC formation, narrow thickness or low connectivity of the diffusion layer, and hence poor accessibility to the active electrode area.

#### 3.2. Ionomer/support phase separation

The ionomer/support interaction may vary significantly for different solvents owing to their different physical and chemical properties. This may affect the distribution and phase separation of ionomer and catalyst support during drying, leading to an inhomogeneous composition of the drop with possibility of local ionomer/support islands. Hence, SEM imaging and EDX of the catalyst inks may provide useful insights into ionomer/catalyst support interaction. SEM images and EDX line mapping of the inks prepared using different solvents have been shown in Figs. 3 and 4. Typical EDX spectrum of an ionomer/catalyst support ink exhibits characteristic peaks corresponding to C, F and S (Fig. 3a) while a magnified view of the ink microstructure at submicron scale appears to be homogeneous as shown in a typical SEM image of Fig. 3b), the homogeneity of ink drops at micron scale seems to be affected significantly by the solvent used (Fig. 3c–f and Fig. 4a–f). EDX line mappings on different ink drops may be used to observe such variations in the ionomer/catalyst support distributions through observation of the relative variation of C/F ratio. Normalized intensities of

C and F X-ray signals suggest the ionomer/catalyst support distribution to be homogeneous for solvents such as IPA, ethanol and glycerol (a one-to-one correspondence between C/F signals throughout the line scan), partially inhomogeneous for solvents such as EG and sulfolene (the C and F intensity peaks appear to be shifted spatially), completely inhomogeneous for solvents such as DMSO, DMF, NMP acetonitrile and acetone. Again, for acetonitrile and acetone solvents, the inhomogeneity arises probably due to incomplete mixing of ionomer in the solvent (the C and F intensity peaks appear randomly with no correspondence). On the other hand, for DMSO, DMF and NMP, it may be attributed to ionomer/catalyst support separation during drying (the ionomer being concentrated at the periphery of the droplet to form a ring) due to poor interaction. Hence, the EDX line mapping of the dried ink drops provides fast and straight-forward evaluation on the ionomer/catalyst support interaction in the dispersion.

### 3.3. Particle size distribution

Distributions of particle sizes in the inks consisting of ionomer and catalyst support dispersed in various solvents provide useful insight of their physical states. Formation of agglomerations can reduce the available surface area significantly, leading to poor performance of the catalyst. As shown in Fig. 5, all of the solvents but acetone show a bimodal or trimodal PSD with submicron sized agglomerations of the ionomer/catalyst support dispersions. This suggests proper dispersion of catalyst support in various solvents. The large agglomerate size in the ink using acetone as solvent might be due to faster vaporization of the solvent leading to agglomeration.

### 3.4. Thermal study

Thermal degradation behavior of different inks in 20% oxygen environment has been depicted in Fig. 6. TG and differential TG (DTG) plots of Fig. 6a and b exhibit significant variation in the thermal degradation behavior of the inks prepared using different solvents. DTG plots exhibit distinct peaks corresponding to ionomer and catalyst support thermal degradation in temperature ranges of 300–400 °C and 550–700 °C respectively. For pure Nafion ionomer, 2 distinct peaks at ~300 and 400 °C may be attributed to respective degradations of the sulfonic groups and the main chain [38], while for pure catalyst support (Vulcan XC 72), the degradation takes place between 650 and 700 °C [39]. Further, for the ionomer/catalyst support inks, peaks corresponding to Nafion ionomer and carbon degradation appear to be shifted from the corresponding temperatures for pure components due to the ionomer/catalyst support interaction. A larger shift of certain peak from its corresponding pure component may be attributed to a stronger ionomer/catalyst support interaction, leading to corresponding change in the bond energies. As shown in Fig. 6b and c (magnified view of Fig. 6c is shown in Fig. 6d), DTG and DSC analysis of different inks suggest varying degrees of peak shifts with IPA and sulfolene having the largest and the lowest values, respectively.

### 3.5. Spectroscopic studies

Spectroscopic studies of the dried inks have been carried out to further investigate the ionomer/catalyst support interaction. IR spectra of the inks prepared using different solvents shown in Fig. 7a exhibit the intense absorption peak at ~1240 cm<sup>-1</sup> and attributed to the asymmetric stretching of  $\text{-SO}_3^-$  groups of Nafion® ionomer [40,41]. Similarly, the Raman spectra of various inks (intensity normalized to D-band maximum), showing D and G bands of carbon respectively at ~1350 and ~1600 cm<sup>-1</sup>, have been depicted in Fig. 6b. Presence of ionomer decreases the G to D band intensity ratio ( $I_G/I_D$ ), suggesting decreased crystallinity [42] or increased disorder [43] probably due to breaking-up of agglomerates. The  $\text{-SO}_3^-$  stretching IR peak and the Raman G-band peaks exhibit significant shift of peak positions for various inks

due to the effect of ionomer/catalyst support interaction.

Here, the observed change of the IR wavenumber ( $\nu$ ) of the  $\text{-SO}_3^-$  stretching peak for the ionomer/support inks as compared to that for the pristine ionomer may be associated to a corresponding change in the S–O bond strength ( $\nu \propto \sqrt{k}$ ; with  $k$  being the force constant) due to ionomer/catalyst support interaction. An increased wavenumber compared to that for the pristine ionomer may be attributed to a shift of electron cloud to  $\text{-S}$  through  $\text{-CF}_2$  and hence an interaction between the support carbon and the main chain (electron transfer from C to F). On the other hand, a decreased wavenumber may be due to a reduced S–O bond strength due to a shift of electron cloud to  $\text{-SO}_3^-$  through the interaction of O with C (electron transfer from C to O). However, in both the cases, charge transfer form C takes place, leading to a  $\delta^+$  charge on C and hence to a modified surface starring. Thus, the observed shift of Raman G-band to higher wavenumbers compared to that for pristine support carbon (1580 cm<sup>-1</sup>) may be attributed to the contribution from the D' band.

## 4. Structure-property correlations

Correlations of the structural parameters obtained from Raman and IR spectroscopy measurements with the ratio of DLC values at scan rates of 1000 and 100 mV/s ( $\text{DLC}_{1000}/\text{DLC}_{100}$ ) have been depicted in Fig. 8. With increasing  $\text{DLC}_{1000}/\text{DLC}_{100}$  ratio, both the spectroscopic parameters, namely the IR shift corresponding to stretching of  $\text{-SO}_3^-$  groups and the Raman G-band peak position exhibit decreasing values. Interestingly, for the Raman shift approaching to the value corresponding to pristine support (1580 cm<sup>-1</sup>), the  $\text{DLC}_{1000}/\text{DLC}_{100}$  ratio approaches to its highest values. This suggests the  $\text{DLC}_{1000}/\text{DLC}_{100}$  ratio to be strongly associated to the ionomer/catalyst support distribution. In view of the EDX analysis of Fig. 3 and the correlations of Fig. 8, the  $\text{DLC}_{1000}/\text{DLC}_{100}$  ratio exhibits high values for either in case of the ionomer/catalyst support separation (DMF, NMP and DMSO) or in case of the uniform coverage (ethanol and IPA). This may be understood from the fact that for the ionomer/catalyst support electrode in liquid electrolyte, proton accessibility may be achieved either through the ionomer (solid electrolyte) or through the liquid electrolyte [44]. Hence, proton accessibility is ensured in both the cases (IPA or DMF) through ionomer or liquid phases. On the other hand, the electron accessibility is provided only through the carbon network. Therefore, inhomogeneous distribution of ionomer and catalyst support making ionomer/catalyst support islands lacks electronic connectivity, leading to higher resistance to DL formation and hence to the lower  $\text{DLC}_{1000}/\text{DLC}_{100}$  ratio.

## 5. Conclusions

Present study highlights the effect of ink dispersion media on the ionomer/catalyst support interaction in the PEMFC electrodes. The SEM imaging and EDX line mapping exhibit formation of different ionomer/catalyst support distributions through the variation of the ionomer/catalyst support dispersion media. The  $\text{DLC}_{1000}/\text{DLC}_{100}$  ratio for different ionomer/carbon support inks reveal different ionomer/carbon support distributions. The study further reveals a negative correlation between the change of DLC with scan rate and the IR shift of  $\text{-SO}_3^-$  stretching peak, which suggests decreasing accessibility of electrochemically active area with increasing ionomer coverage of the support. Hence, the spectroscopic and microscopic techniques have been supplemented the electrochemical ones successfully to investigate the ionomer/support interface in a PEMFC catalyst layer. The dependence of support/ionomer distributions on the ink solvent suggests suitability of solvents such as isopropanol where both electronic as well as protonic connectivities can be insured. On the other hand, inks prepared using solvents such as DMF, despite their high DLC values, may not be preferred due to inhomogeneous ionomer/support distribution. Consideration of ionomer/catalyst support interaction may be of significant importance towards optimizing the ionomer/catalyst interface

structure in PEMFC catalyst layer.

## Acknowledgement

The authors appreciate Dr. Martin A.B. Hedegaard and Ph.D. fellow Anders Runge Walther for their assistance in Raman spectroscopy. The authors appreciate Associate Professor Per Morgen for assistance in SEM and EDX. The authors appreciate the financial support from VILLUM FONDEN blokstipendier, UpCat (ForskEL J.No 2015-1-12315), and from the Danish Council for Strategic Research, Innovation Fond Denmark, through the 4M Centre (J.No 12-132710).

## References

- [1] D. Banham, S. Ye, Current status and future development of catalyst materials and catalyst layers for proton exchange membrane fuel cells: an industrial perspective, *ACS Energy Lett.* 2 (2017) 629–638.
- [2] M. Shaneeth, S. Basu, S. Aravamuthan, PEM fuel cell cathode catalyst layer durability: an electrochemical spectroscopic investigation, *Chem. Eng. Sci.* 154 (2016) 72–80.
- [3] S. Litster, G. McLean, PEM fuel cell electrodes, *J. Power Sources* 130 (2004) 61–76.
- [4] M. Shao, Q. Chang, J.-P. Dodelet, R. Chenitz, Recent advances in electrocatalysts for oxygen reduction reaction, *Chem. Rev.* 116 (2016) 3594–3657.
- [5] S. Chabi, M. Kheirmand, Electrocatalysis of oxygen reduction reaction on Nafion/platinum/gas diffusion layer electrode for PEM fuel cell, *Appl. Surf. Sci.* 257 (2011) 10408–10413.
- [6] J. Stacy, Y.N. Regmi, B. Leonard, M. Fan, The recent progress and future of oxygen reduction reaction catalysis: a review, *Renew. Sustain. Energy Rev.* 69 (2017) 401–414.
- [7] S. Sui, X. Wang, X. Zhou, Y. Su, S. Riffat, C.-j. Liu, A comprehensive review of Pt electrocatalysts for the oxygen reduction reaction: nanostructure, activity, mechanism and carbon support in PEM fuel cells, *J. Mater. Chem. 5* (2017) 1808–1825.
- [8] J. Marquis, M.O. Coppens, Achieving ultra-high platinum utilization via optimization of PEM fuel cell cathode catalyst layer microstructure, *Chem. Eng. Sci.* 102 (2013) 151–162.
- [9] A. Kulkarni, S. Siahrostami, A. Patel, J.K. Nørskov, Understanding catalytic activity trends in the oxygen reduction reaction, *Chem. Rev.* 118 (5) (2018) 2302–2312.
- [10] S.M. Andersen, Nano carbon supported platinum catalyst interaction behavior with perfluorosulfonic acid ionomer and their interface structures, *Appl. Catal. B Environ.* 181 (2016) 146–155.
- [11] S.M. Andersen, M. Borghei, R. Dhiman, H. Jiang, V. Ruiz, E. Kauppinen, E. Skou, Interaction of multi-walled carbon nanotubes with perfluorinated sulfonic acid ionomers and surface treatment studies, *Carbon* 71 (2014) 218–228.
- [12] S.M. Andersen, R. Dhiman, M.J. Larsen, E. Skou, Importance of electrode hot-pressing conditions for the catalyst performance of proton exchange membrane fuel cells, *Appl. Catal. B Environ.* 172–173 (2015) 82–90.
- [13] S.M. Andersen, L. Grahl-Madsen, Interface contribution to the electrode performance of proton exchange membrane fuel cells – impact of the ionomer, *Int. J. Hydrogen Energy* 41 (2016) 1892–1901.
- [14] K. Artyushkova, M.J. Workman, I. Matanovic, M.J. Dzara, C. Ngo, S. Pylypenko, A. Serov, P. Atanassov, Role of surface chemistry on catalyst/ionomer interactions for transition metal–nitrogen–carbon electrocatalysts, *ACS Appl. Energy Mater.* 1 (2018) 68–77.
- [15] J. Chlistunoff, B. Pivovar, Effects of ionomer morphology on oxygen reduction on Pt, *J. Electrochem. Soc.* 162 (2015) F890–F900.
- [16] Q. He, N.S. Suraweera, D.C. Joy, D.J. Keffer, Structure of the ionomer film in catalyst layers of proton exchange membrane fuel cells, *J. Phys. Chem. C* 117 (2013) 25305–25316.
- [17] T.-H. Kim, J.-Y. Yi, C.-Y. Jung, E. Jeong, S.-C. Yi, Solvent effect on the Nafion agglomerate morphology in the catalyst layer of the proton exchange membrane fuel cells, *Int. J. Hydrogen Energy* 42 (2017) 478–485.
- [18] Y.-C. Park, K. Kakinuma, H. Uchida, M. Watanabe, M. Uchida, Effects of short-side-chain perfluorosulfonic acid ionomers as binders on the performance of low Pt loading fuel cell cathodes, *J. Power Sources* 275 (2015) 384–391.
- [19] Y.-C. Park, H. Tokiwa, K. Kakinuma, M. Watanabe, M. Uchida, Effects of carbon supports on Pt distribution, ionomer coverage and cathode performance for polymer electrolyte fuel cells, *J. Power Sources* 315 (2016) 179–191.
- [20] F. Yang, L. Xin, A. Uzunoglu, Y. Qiu, L. Stanciu, J. Ilavsky, W. Li, J. Xie, Investigation of the interaction between nafion ionomer and surface functionalized carbon black using both ultrasmall angle X-ray scattering and cryo-TEM, *ACS Appl. Mater. Interfaces* 9 (2017) 6530–6538.
- [21] X.-y. Zhang, Y.-h. Ding, Thickness-dependent structural and transport behaviors in the platinum-Nafion interface: a molecular dynamics investigation, *RSC Adv.* 4 (2014) 44214–44222.
- [22] B. Jeong, J.D. Ocon, J. Lee, Electrode architecture in galvanic and electrolytic energy cells, *Angew. Chem. Int. Ed.* 55 (2016) 4870–4880.
- [23] A. Ignaszak, S. Ye, E. Gyenge, A study of the catalytic interface for O<sub>2</sub> electro-reduction on Pt: the interaction between carbon support meso/microstructure and ionomer (nafion) distribution, *J. Phys. Chem. C* 113 (2009) 298–307.
- [24] S.M. Andersen, E. Skou, Electrochemical performance and durability of carbon supported Pt catalyst in contact with aqueous and polymeric proton conductors, *ACS Appl. Mater. Interfaces* 6 (2014) 16565–16576.
- [25] T.-H. Huang, H.-L. Shen, T.-C. Jao, F.-B. Weng, A. Su, Ultra-low Pt loading for proton exchange membrane fuel cells by catalyst coating technique with ultrasonic spray coating machine, *Int. J. Hydrogen Energy* 37 (2012) 13872–13879.
- [26] M.K. Debe, Novel Catalysts, Catalysts Support and Catalysts Coated Membrane Methods, *Handbook of Fuel Cells*, John Wiley & Sons, Ltd, 2010.
- [27] N. Rajalakshmi, K.S. Dhatathreyan, Catalyst layer in PEMFC electrodes—fabrication, characterisation and analysis, *Chem. Eng. J.* 129 (2007) 31–40.
- [28] S. Thanasilp, M. Hunsom, Effect of MEA fabrication techniques on the cell performance of Pt–Pd/C electrocatalyst for oxygen reduction in PEM fuel cell, *Fuel* 89 (2010) 3847–3852.
- [29] A.J. Bard, L.R. Faulkner, *Electrochemical Methods: Fundamentals and Applications*, Wiley, New York, 2001.
- [30] K. Karan, PEFC catalyst layer: recent advances in materials, microstructural characterization, and modeling, *Curr. Opin. Electrochem.* 5 (2017) 27–35.
- [31] H. Fathi, A. Raoof, S.H. Mansouri, Insights into the role of wettability in cathode catalyst layer of proton exchange membrane fuel cell: pore scale immiscible flow and transport processes, *J. Power Sources* 349 (2017) 57–67.
- [32] Y. Zhang, A. Smirnova, A. Verma, R. Pitchumani, Design of a proton exchange membrane (PEM) fuel cell with variable catalyst loading, *J. Power Sources* 291 (2015) 46–57.
- [33] M.K. Cho, H.-Y. Park, S.Y. Lee, B.-S. Lee, H.-J. Kim, D. Henkensmeier, S.J. Yoo, J.Y. Kim, J. Han, H.S. Park, Y.-E. Sung, J.H. Jang, Effect of catalyst layer ionomer content on performance of intermediate temperature proton exchange membrane fuel cells (IT-PEMFCs) under reduced humidity conditions, *Electrochim. Acta* 224 (2017) 228–234.
- [34] R. Barbosa, B. Escobar, U. Cano, J. Ortega, V.M. Sanchez, Multiscale relationship of electronic and ionic conduction efficiency in a PEMFC catalyst layer, *Int. J. Hydrogen Energy* 41 (2016) 19399–19407.
- [35] M. Schulze, C. Christenn, XPS investigation of the PTFE induced hydrophobic properties of electrodes for low temperature fuel cells, *Appl. Surf. Sci.* 252 (2005) 148–153.
- [36] D.A. Brownson, C.E. Banks, *The Handbook of Graphene Electrochemistry*, Springer, 2014.
- [37] P.K. Sow, Z. Lu, H. Talebian, L. Damron, W. Mérida, Double layer capacitance measurements to characterize the water intrusion into porous materials, *J. Phys. Chem. C* 120 (2016) 24794–24802.
- [38] M. Feng, R. Qu, Z. Wei, L. Wang, P. Sun, Z. Wang, Characterization of the thermolysis products of Nafion membrane: a potential source of perfluorinated compounds in the environment, *Sci. Rep.* 5 (2015) 9859.
- [39] D. Santiago, G.G. Rodríguez-Calero, H. Rivera, D.A. Tryk, M.A. Scibioh, C.R. Cabrera, Platinum electrodeposition at high surface area carbon vulcan-XC-72r material using a rotating disk-slurry electrode technique, *J. Electrochem. Soc.* 157 (2010) F189–F195.
- [40] R. Kumar, C. Xu, K. Scott, Graphite oxide/Nafion composite membranes for polymer electrolyte fuel cells, *RSC Adv.* 2 (2012) 8777–8782.
- [41] X. Teng, C. Sun, J. Dai, H. Liu, J. Su, F. Li, Solution casting Nafion/polytetrafluoroethylene membrane for vanadium redox flow battery application, *Electrochim. Acta* 88 (2013) 725–734.
- [42] L.G. Cançado, K. Takai, T. Enoki, M. Endo, Y.A. Kim, H. Mizusaki, A. Jorio, L.N. Coelho, R. Magalhães-Paniago, M.A. Pimenta, General equation for the determination of the crystallite size La of nanographite by Raman spectroscopy, *Appl. Phys. Lett.* 88 (2006) 163106.
- [43] R. Sharma, K.K. Kar, Effects of structural disorder and nitrogen content on the oxygen reduction activity of polyvinylpyrrolidone-derived multi-doped carbon, *J. Mater. Chem. 3* (2015) 11948–11959.
- [44] R. Sharma, S.M. Andersen, Quantification on degradation mechanisms of polymer electrolyte membrane fuel cell catalyst layers during an accelerated stress test, *ACS Catal.* 8 (2018) 3424–3434.